CNT FIBER VEIL INTERLEAVED CARBON FIBER/EPOXY LAMINATE COMPOSITE

Yunfu Ou [1,2,*], Carlos González [1,2] and Juan José Vilatela [1]

[1] IMDEA Materials - Madrid Institute for Advanced Studies of Materials, c/ Eric Kandel, 2 - Parque Científico y Tecnológico TecnoGetafe, 28906, Getafe, Madrid, Spain.
Website: http://www.materiales.imdea.org/. Email: yunfu.ou@imdea.org

[2] Polytechnic University of Madrid, Department of Material Science, E. T. S. de Ingenieros de Caminos, Ciudad Universitaria, 28040, Madrid, Spain

Keywords: CNT veils, interlaminar property, carbon fiber, toughness

ABSTRACT

Though fiber reinforced polymer (FRP) composites are widely utilized in structural components due to their favorable mechanical properties, delamination between reinforcing plies remains a problematic, limiting more widespread applications of FRPs. Carbon nanotubes (CNTs) carry the promise of enhancing this poor out-of-plane mechanical performance. In this work, macroscopic CNT veils with controlled nano-meso structure were drawn directly from the gas-phase using a semi-industrial process and then integrated into woven and unidirectional carbon fiber (CF)/epoxy matrix composites utilizing vacuum assisted resin transfer moulding (VARTM) and hot press approaches, respectively. Interlaminar fracture toughness (ILFT) of the resultant composites was determined in Mode-I (opening mode) and Mode-II (shearing mode) conditions. Crack propagation and interlaminar toughening mechanisms were systematically analyzed by means of optical microscope, SEM, and Raman analysis. The mechanical testing results showed that mode I ILFT of woven fabric/epoxy laminate was improved as much as 60% when interleaving as-received fluffy CNT veils. Fracture analysis revealed that interlaminar crossing plays a dominant role amongst toughening mechanisms. In comparison, interleaving as-received CNT veils into unidirectional CFRP system led to an increase of Mode II ILFT (22%) but a significant decrease of Mode I ILFT (-64%).

1 INTRODUCTION

The mechanical performance of FRP composites arises from the synergistic effect of its constituent materials. This has been the motivation for incorporating nanomaterials with tensile strength and modulus beyond current macrofiber reinforcements in order to impart these impressive properties. For example, nano-scale reinforcement using nanofillers like CNTs in between the plies of a composite offers the opportunity to reinforce the interlaminar bonding with minimal weight penalty and effectively avoids reductions in in-plane properties. The presence of CNTs can provide reinforcement in the z-direction (perpendicular to the ply thickness), and arrest crack growth by “bridging” the crack between the plies. These hierarchical composites can further bear high electrical conductivity or piezoresistivity if proper structural and interfacial organization are achieved [1].

Several approaches for integrating CNTs into FRP structural composites have been studied [2]. Among them, dispersing CNTs entirely throughout the composite matrix seems to be the most economically compatible and facile route. The main problem of this approach is that the viscosity of a CNT-modified matrix increases dramatically with increasing CNT mass/volume fracture, leading to incomplete matrix infusion [3]. Also, it is difficult to get a homogeneous dispersion of CNTs into final laminate by means of infusion [4].

Assembling micro CNTs into macro fiber veils [5] could solve the abovementioned problems of increased viscosity and inhomogeneous dispersion, as these veils can be easily and readily deposited in between the reinforcing fiber plies before infusion. Thus, the viscosity of the resin is not influenced during the infusion process. What is more, CNT fibers have an unusual yarn-like structure with an accessible surface area several orders of magnitude higher than that of a traditional fiber. The free

space between bundles in the CNT is then able to be taken up by non cross-linked resins via capillary force [8].

In this work, continuous macroscopic fibers of CNTs were drawn from the gas-phase during their growth by chemical vapor deposition, and then integrated into unidirectional and woven CFRP composites using a facile and scalable approach. Thus, a hierarchical structure was manufactured, as shown in **Figure 1**. The critical energy release rate of mode I and II delamination (G_{IC} and G_{IIC}) of the CNT toughened CFRP composites were then compared with that of conventional CFRPs combined with a deep analysis of their toughening mechanisms.

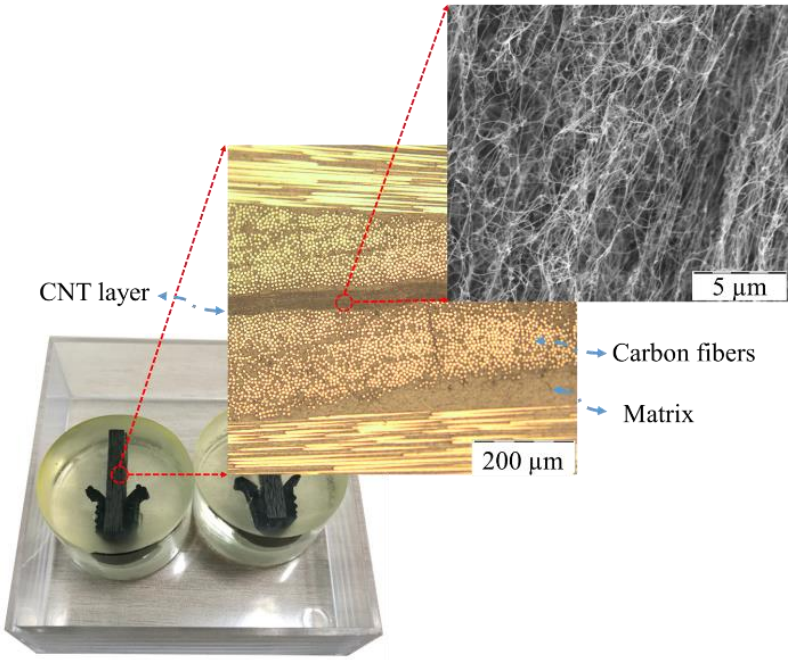

Figure1: The hierarchical structure of woven CF/epoxy composites interleaved with CNT veils.

2 EXPERIMENTAL

2.1 Materials

CNT fibers were synthesized by the direct spinning process from the gas-phase during growth of CNTs by floating catalyst chemical vapor deposition (FFCVD [5]), utilizing ferrocene as iron catalyst, thiophene and butanol as sulfur catalyst promoter and carbon source, respectively. The reaction was carried out in the hydrogen atmosphere at 1250 °C with precursor feed rate of 5 mL h^{-1} and a winding rate of 20 m min^{-1}. The carbon fabrics used in this study was provided by HEXCEL with a weave style of 5H satin. The CNT fibers were continuously drawn out at the exit of the furnace and directly deposited onto the surface of a piece of carbon fabric/prepreg which was wrapped on a rotating spindle (D = 10 mm). Winding time of CNT fibers was set as 0.5 h, which gave an areal density of 0.8 g/m^2. DERAKANE 8084 was chosen as matrix which is an elastomer-modified bisphenol-A epoxy vinyl ester resin for structural applications and provided by Ashland Inc. Both the MEKP hardener and Cobalt octoate catalyst were available from Plastiform S.A. By using the recommended concentration of precursors (100:1.5:0.3), the matrix will reach its gel point after 30–60 min. Unidirectional carbon fiber prepregs (HexPly® 8552/34%/UD 194/AS4/1219MM) were also purchased from HEXCEL.

2.2 Laminate manufacturing

Both VARTM and hot press methods were employed to integrate CNT veils into CFRP structural composites, as schematically illustrated in **Figure 2**. For the former, 8 woven fabrics were used. Two layers of infusion media were placed onto the upper and bottom surfaces to promote the resin flow, to guarantee complete wet-out of the preform and to eliminate dry spots and voids. The length of infusion

media was designed to be 30 mm shorter than that of fabric in order to slow down the speed of flow front before it reaches the outlet and leave enough time to complete infiltration of z-direction. After completing the infusion process, the inlet and outlet of the system was closed off and cured at room temperature (RT) for 24 hours, followed by a post curing step at 60°C for 2 hours. For the latter, 1 panels of 20 plies unidirectional carbon fiber prepreg (280 mm × 280 mm) were laid up with a nominal thickness of 3.65 mm. A 25 mm-thick Teflon film was inserted as a crack starter in the middle of the panel, serving as the delamination plane for Mode I test. Hot-Plate Press machine (LabPro 400, Fontijne Presses) was then used to consolidate laminate panel from pre-impregnated sheets of fibre-reinforced composites by simultaneous application of pressure (up to 7 bar) and heat (up to 180 ºC).

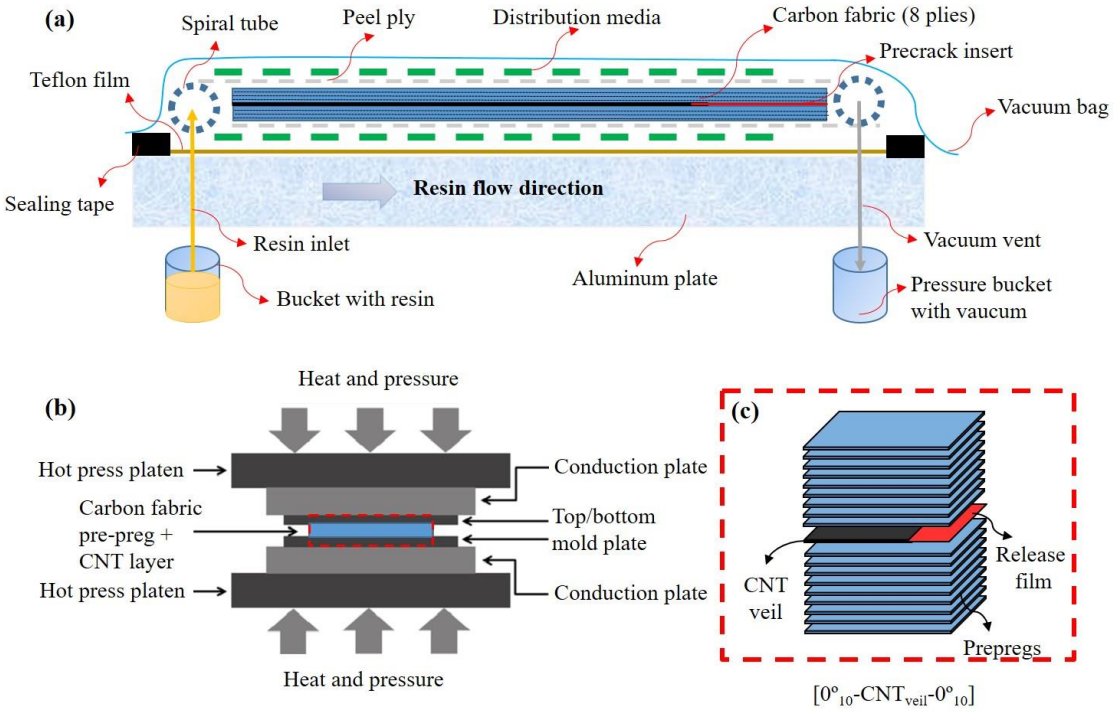

Figure 2: Schematic illustrations of (a) optimized VARTM method and (b) hot press method.

2.3 Mechanical characterization

For Mode I, a Double Cantilever Beam (DCB) test was chosen, whereas for Mode II a 4-point End-Notched Flexure (4ENF) setup was adopted. Specifically, the DCB tests were carried out in accordance with ASTM Standard D5528-01 [6]. Measurements were conducted in a standard testing machine (Instron 3384) at loading rate of 1 mm/min. Force was detected by utilizing a 500 N load cell and the displacement recorded by load frame, both of which were digitally stored by the machine. Modified Beam Theory (MBT) method was employed to calculate the Mode I fracture toughness (G_{IC}) and the strain energy release rate (G_I) can be obtained by the following equation:

$$G_I = \frac{3*F*\delta}{2*w*(a+|\Delta|)} \quad (1)$$

where F is the load; δ is the load point displacement; w is the sample width, and a is the crack length from the load point. The coefficient **Δ** could be determined by plotting the cube root of the compliance (displacement divided by force) against the crack length.

For the 4ENF tests, an initial crack in the specimens were first generated by subjecting the specimen to Mode I opening loading. 4-point bending tests were then carried out on Instron 3384 with a 10 kN load cell, at a displacement rate of 0.25 mm/min. The acquisition rate was set as 10 data points per second. As in Mode I test, crack growth was visually observed and listed in an experimental

sheet. Evaluation of the fracture toughness (G_{IIC}) of the 4ENF specimens is based on the compliance calibration method [7], as given by equation below:

$$G_{II} = \frac{F^2 m}{2w} \quad (2)$$

where m is the slope calculated by a plot of compliance (C) against delamination length (a), After fracture, $F = F_c$, and $G_{II} = G_{IIC}$.

2.4 Other characterizations

Scanning electron microscope (SEM) and optical microscope were used to investigate the morphology of CNT fiber veils as well as the fracture surfaces of the laminates. Raman spectroscopy (530 nm wavelength) analysis was also performed to identify constitutents at the fracture surface.

3 RESULTS AND DISCUSSION

3.1 CNT veil/woven fabric/epoxy (VARTM)

3.1.1 Mode I testing and fracture surface analysis

Pristine and CNT veil-interleaved woven composites were produced with the 5H Satin weave fabrics. Though the load-extension curves of woven composites always display stick-slip crack propagation behavior, as shown in **Figure 3a**, the data can still be utilized to generate R-curves [8].

There is moderate fiber bridging in the pure woven laminates, resulting in a relatively flat R-curve, which is in line with similar systems [9]. For the control samples without CNT veils, the difference between $G_{IC,ini}$ and $G_{IC,prop}$ is marginal, especially when compared with the differences observed in unidirectional fiber reinforced composites [9, 10]. Incorporation of the low-density, as-produced CNT veils, produces a sharp rise in the R-curve, with the propagation value of fracture toughness ($G_{IC,\,prop}$) increasing up to ~50% compared with the initiation value ($G_{IC,\,ini}$) due to a hierarchical fiber-bridging toughening mechanism). Remarkably, the average values of $G_{IC,\,prop}$ for as-produced CNT samples are 60% higher compared with the corresponding value of the baseline material. In contrast, the densified veils produced a 28.4% decrease of $G_{IC,\,prop}$.

The fracture surfaces of tested specimen were examined by SEM as displayed in **Figure 3d**, **e** and **f**. Typical features of brittle Mode-I fracture were observed in the reference specimen (**Figure 3d**), showing a very smooth matrix fracture surface and no fiber-bridging, in line with its flat R-curve (**Figure 3b**). When integrating fluffy as-received CNT veils into resin-rich layer, the case is totally different. Overall the interlayer is modified by the addition of CNTs, which participate in delaying the crack initiation or hindering the crack propagation by deflection, blocking or crack bridging. These mechanisms help increase the absorption of the applied energy. The extensive CNT breaking and pull-out, as shown in micrographs of **Figure 3e**, are well in agreement with the prior explained toughening mechanisms. In comparison, the fracture surface of laminates interleaved with densified CNT veils (**Figure 3f**) shows peeling of the CNT interleaf layer. No carbon fiber was easily detected at fracture surface, which indicates that the densified CNT layer guided the crack and hindered the formation of carbon fiber bridging. The fracture energy obtained in this case can be endorsed to the intrinsic fracture energy of the CNT layer in the absence of other superior toughening mechanisms.

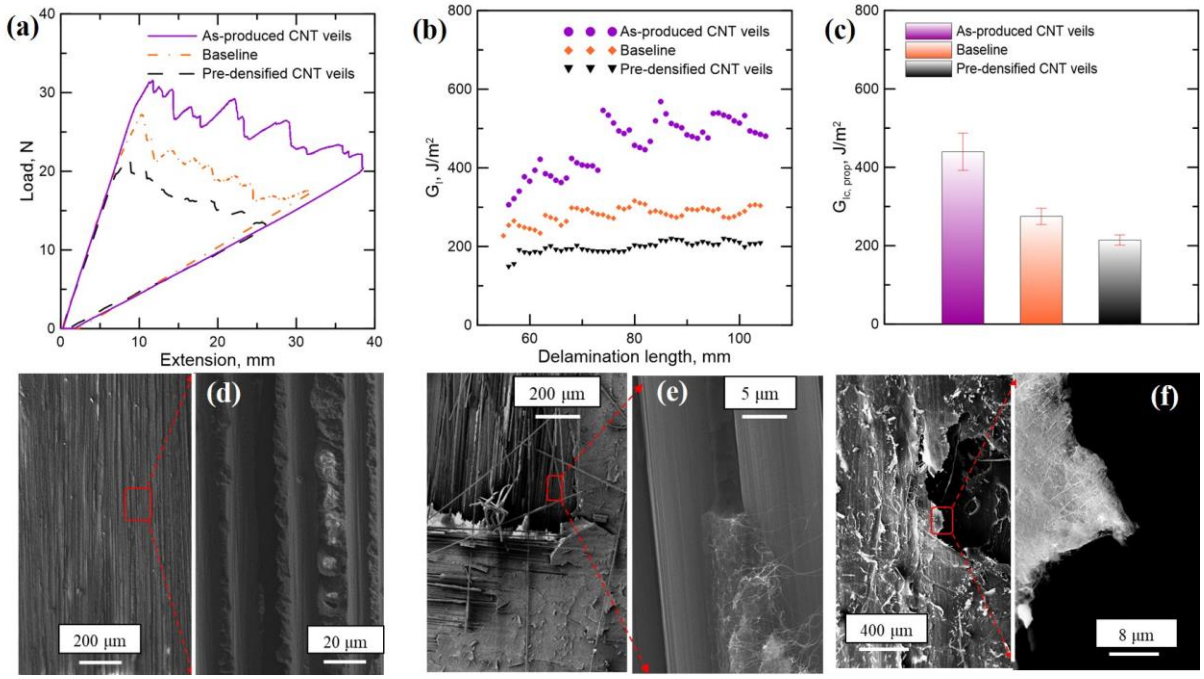

Figure 3: Representative (a) Load-extension curves and (b) R-curves of specimens with and without CNT veils; (c) comparison of Mode I interlaminar fracture toughness for CNT-interleaved composites (as-produced and pre-densified CNT veils) and baseline (without CNT veils). Comparison of fracture surfaces: (d) Control sample without CNT veils; (e) sample interleaved with as-produced CNT veils and (f) sample containing pre-densified CNT veils.

3.1.2 Crack propagation

Toughening effect, to a considerable degree, depends on crack behavior. Several surface analysis technologies were used in order to get a deep insight into the crack initiation and propagation behaviors as well as the toughening logics. As represented in **Figure 4a**, three distinct regions were observed on the whole fracture surface, named as shiny, grey and dark part respectively. By means of Raman spectroscopy analysis, main ingredient of each part could be readily determined, and then how cracks initiate and propagate can be easily imaged.

Specifically, dark and grey part can be readily recognized as CNT regions when comparing their Raman spectra with that of CNT veils, while shiny part display a typical Raman spectra of carbon fiber [11]. This relationship between color and material was further confirmed by High resolution SEM pictures. As shown in **Figure 4b (T2)**, shiny region actually consists of pure carbon fibers. Those fibers debonded from CNT-rich Resin, left substantial dents on the counterpart (**B2,** grey region). Thus it is of confidence to speculate that crack move forwards in the interface of carbon fabric layer and CNT layer (see **Figure 4b (II)**). In addition, the dark part in one piece of sample always corresponds to a dark region in its counterpart, and the SEM pictures proved that both part shared the similar fracture morphologies with massive breakage/pullouts of CNTs (see **Figure 4b (T1&B1)**). Crack, in this case, exclusively passes though the CNT layer, as depicted in **Figure 4b (I).** Following this logic, the propagation routes of cracks in whole area of interest (AOI) could be unveiled, simply based on the apparent color of fracture surfaces.

Figure 5 presents the fracture surfaces of two different samples and schematics of the different crack propagation paths. It manifested that delaminations in CNT-toughened sample with poor fracture toughness progress almost exclusively within nano-toughened interlayer. The energy required for such failure will depend on the adhesion of the CNT with the matrix resin, however, this kind of bonding in this sample was proved to be weak due to the poor infiltration of resin among CNTs. In comparison, the delaminations in sample with excellent energy-consuming behavior show regular crossings of the interlaminar region through the nano-toughened interlayer. This saw-like interlaminar crossings result in a crack not only through the nanotoughened epoxy (causing nano-scale bridgings), but also

entangled with woven fabric (triggering carbon fiber bridgings), which significantly enhances the interlaminar fracture toughness.

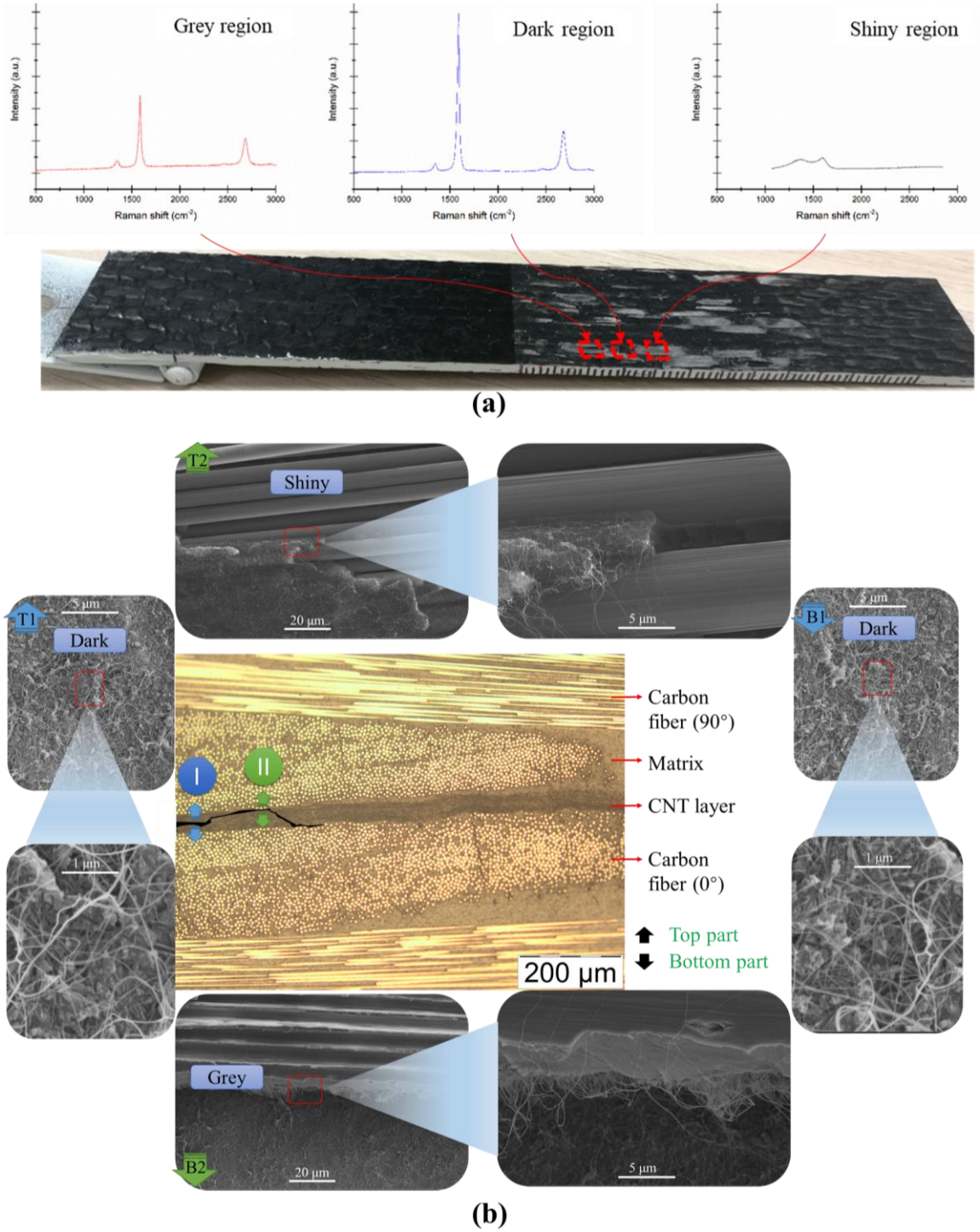

Figure 4: (a) Three different morphologies (i.e. grey, dark and shiny) identified on the fracture surface of laminates reinforced with as-produced CNT veils and their respective Raman spectra. (b) Cross-sectional image of this laminate with a crack propagating either within CNT-toughened interlayer (I) or along the interface between CNT layer and carbon fiber layer (II). T1 and B1 display the typical fracture surfaces at the position (I), which share remarkable similarities with massive breakage or pullouts of CNTs; T2 and B2 show the representative morphologies at the position (II), detecting substantial debondings of macro carbon fibers and pullouts of CNTs.

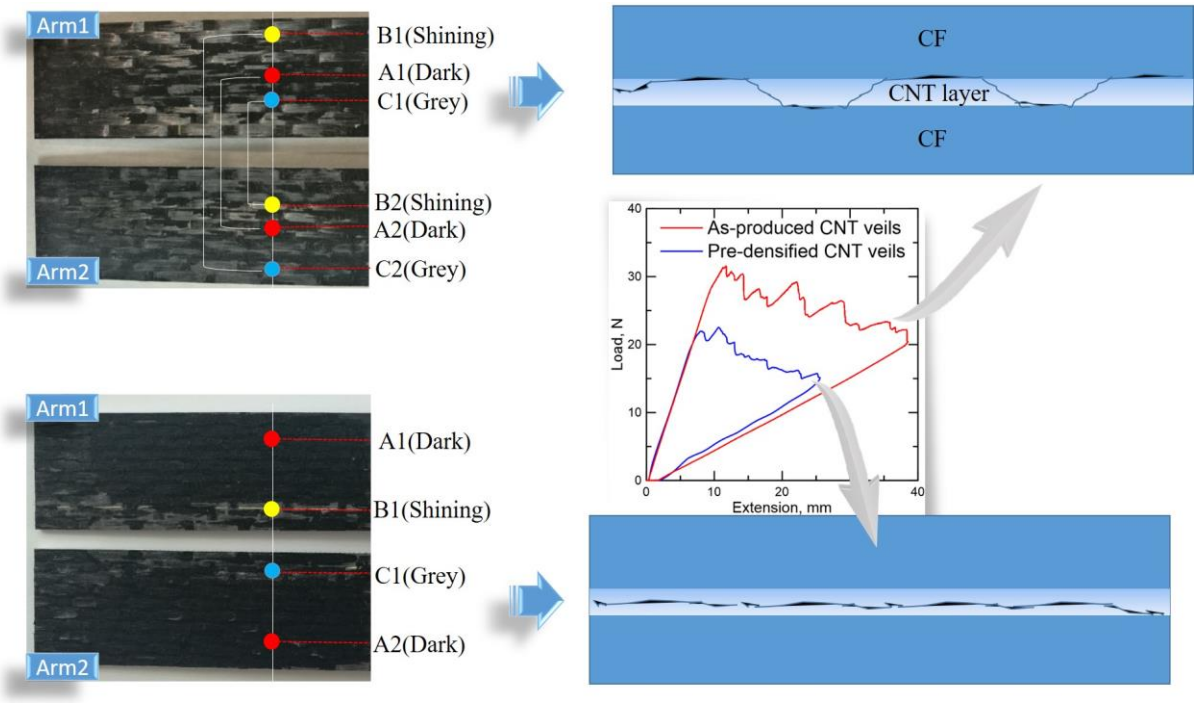

Figure 5: Fracture surfaces of the two types of composites with CNT veil interleaves. Increases in Mode I fracture toughness correspond to a saw-like crack path alternating between cohesive and adhesive failure in samples with low-density as-produced veils. Pre-densified veils reduced fracture toughness and failed exclusively cohesively.

3.2 CNT veil/unidirectional fabric/epoxy (Hot press)

3.2.1 Mode I testing and fracture surface analysis

In this section, baseline and CNT veils interleaved composite laminates were manufactured with AS4/8552 unidirectional prepregs. All the samples exhibited a stable crack propagation, which advanced smoothly without jumps after onset of failure. This is visible from the load-displacement curves, as shown in **Figure 6a**. In comparison, the load-displacement curves of woven fabric (such as twill [9, 12], plain weave[13] or Satin[14]) laminates often show stick-slip crack growth behavior. Also, there is a relatively large increase in G_I with increasing crack growth, leading to a remarkable difference between $G_{IC,ini}$ and $G_{IC,prop}$, which is mainly due to carbon fibers bridging the DCB specimen halves. This is confirmed by the visual observation during the test and the high resolution SEM images of the fracture surfaces of baseline samples, as shown in **Figure 7 a** and **b**. For samples with CNT veils, the load-displacement curves are quite divergent (**Figure 6a**), which could be attributed to the intrinsic anisotropy and randomness of CNT veils. In addition, the rising R-curve behavior was not observed among those samples (**Figure 6b**), Apparently, the presence of the CNT fiber veils in the interlayer region between UD plies blocked the formation of a carbon fiber bridging zone resulting in relatively flat R-curves. It is noteworthy that the $G_{IC,\,prop}$ value of samples interleaved with as-produced CNT veils on average decreased by as high as 64% compared with the baseline. **Figure 7c** and **d** showed typical fracture surfaces of samples with CNT veils, noting that there was no micro carbon fiber bridging triggered. The crack almost exclusively propagated along the CNT-rich interlayer, corresponding to a cohesive failure. A similar behavior is observed in composites produced with CNT veils produced semi-industrially, which are supplied as densified free-standing sheets [14].

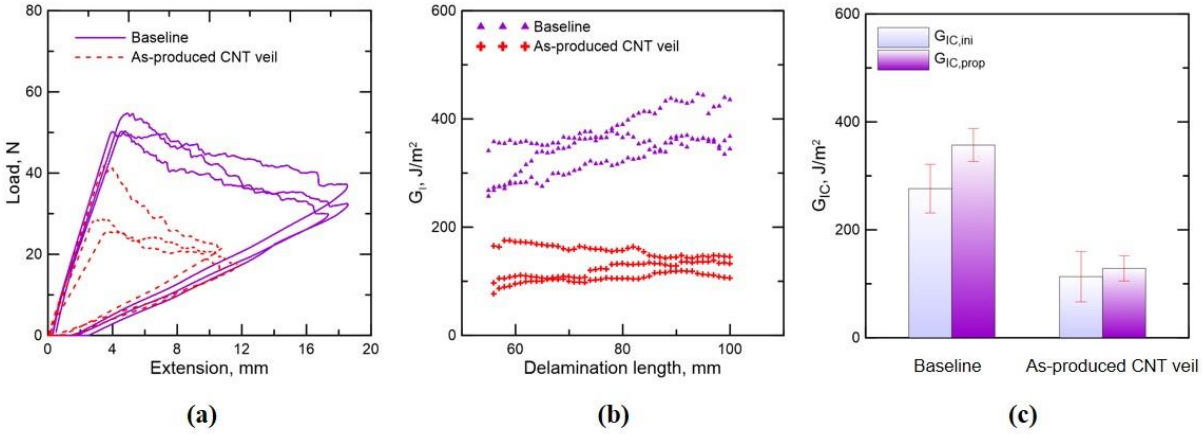

Figure 6: Representative (a) load-extension curves and (b) R-curves of specimens with and without CNT veils in Mode I test; (c) comparison of Mode I ILFT for CNT-interleaved composites and baseline (without CNT veils).

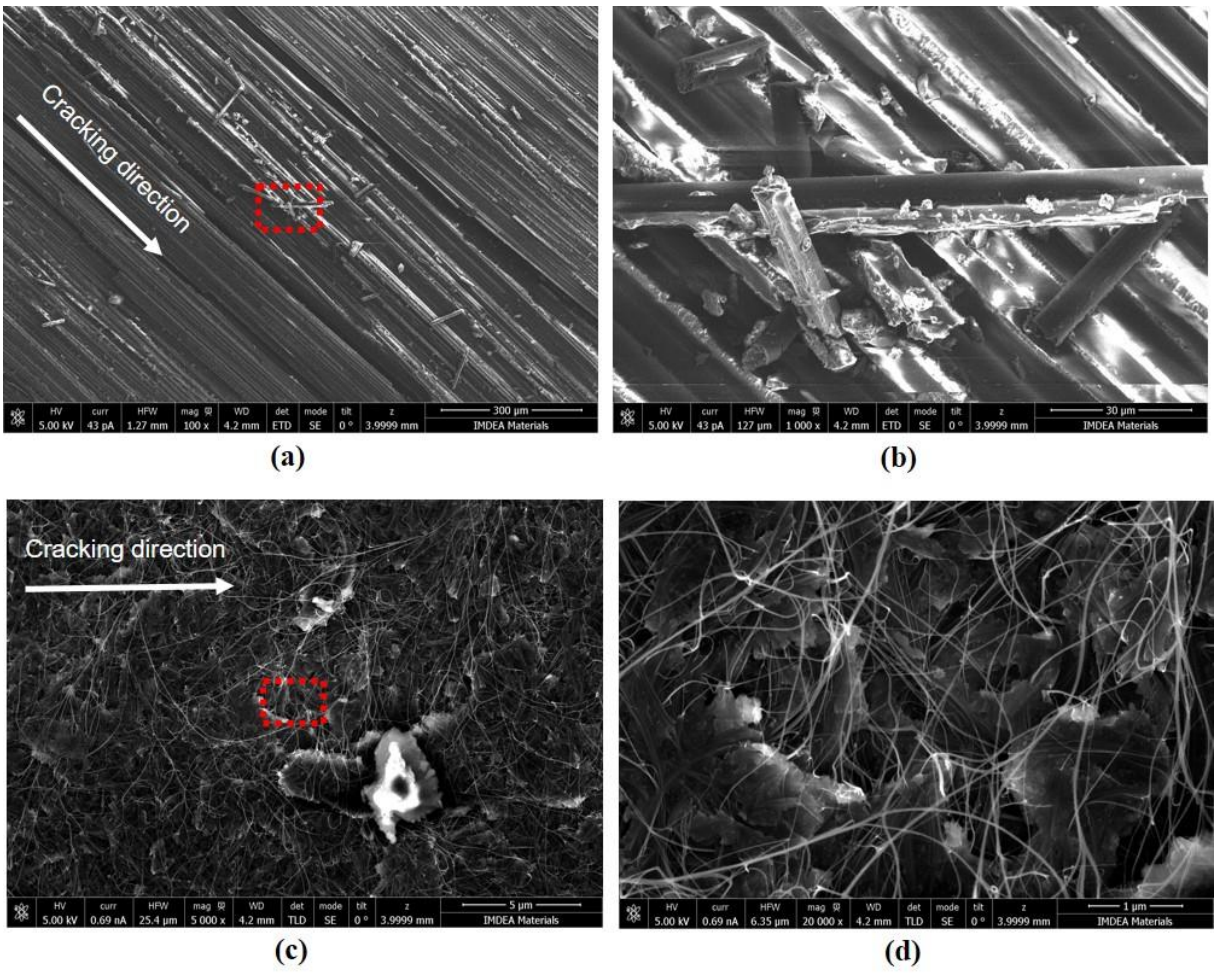

Figure 7: Comparison of fracture surfaces under Mode I loading case: (a) Control sample without CNT veils; (c) sample interleaved with as-produced CNT veils. (b) and (d) are enlarged pictures of marked regions within dashed boxes.

3.2.2 Mode II testing and fracture surface analysis

The three-point bend end-notched flexure (ENF) test is perhaps the most commonly used test for determining the mode II delamination toughness of laminated composites[15, 16]. However, under this test condition, the crack growth is not stable and therefore only one data point per sample can be obtained. Then, a modified loading condition, an end-notched sample subjected to four-point bending (4ENF), was proposed [17]. It was reported that crack growth in 4ENF test was stable and it is possible to get several data points from each single test [17, 18]. In view of this, 4ENF test protocol was adopted here in order to obtain a complete resistance curve (R-curve). To our surprise, the crack growth was still observed to be unstable (see **Figure 8a**). Furthermore, the baseline and samples interleaved with CNT veils both achieved surprisingly high Mode II fracture toughness, i.e. 1560±69 and 1912±115 J/m^2, respectively, much larger than respective Mode I values. The unstable cracking behavior, therefore, might be ascribed to the ultrahigh accumulated energy under 4-point bending condition. Interestingly, the G_{IIC} value of as-produced CNT samples on average increased by as high as 22% compared with the baseline (**Figure 8b**). By scrutinizing the fracture surfaces as displayed in **Figure 9**, we can find that, for baseline, there existed massive debonding between carbon fibers and resin. The ILFT in this case strongly depends on the bond strength between carbon fiber and resin. For CNT interleaved samples, a large amount of CNTs were highly aligned and stretched (**Figure 9d①**), participating in the energy dissipation under mode II fracture process. Surprisingly, unlike Mode I case, some carbon fibers were also observed in the fracture surface (**Figure 9d②**), indicating that the crack in this case propagates not only within the CNT layer, but also crosses through the CNT rich region, propagates along the interface of CNT layer and CF layer. Thus sufficient regions were involved into energy dissipation process, leading to a higher ILFT.

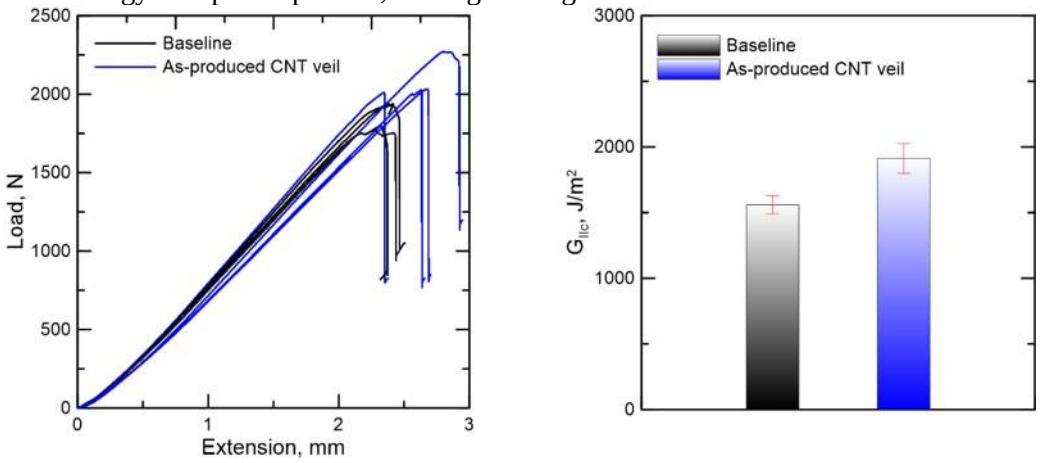

Figure 8: (a) Representative Load-displacement curves of specimens with and without CNT veils in Mode II test and (b) Comparison of Mode II ILFT for CNT-interleaved composites and baseline (without CNT veils).

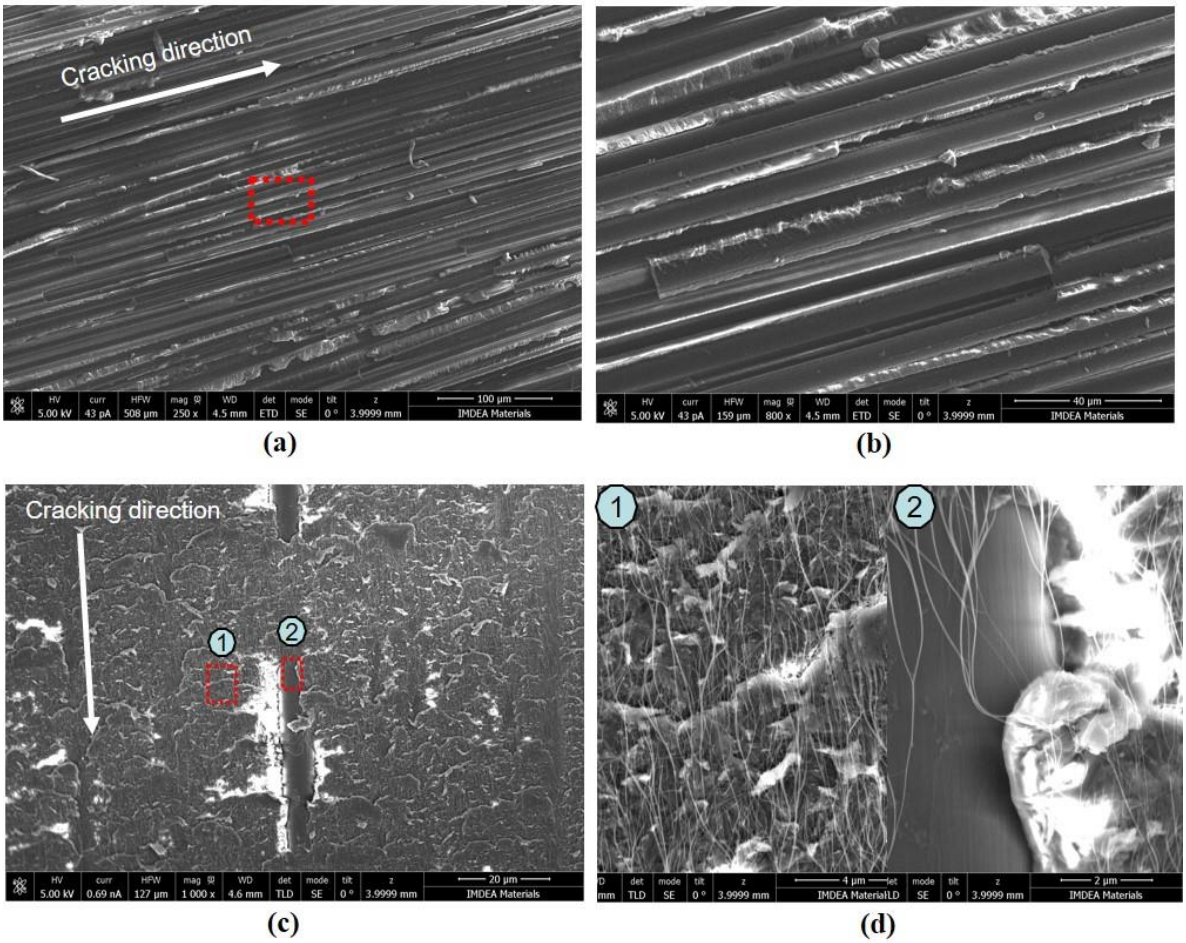

Figure 9: Comparison of fracture surfaces under Mode II loading case: (a) Control sample without CNT veils; (c) sample interleaved with as-produced CNT veils. (b) and (d) are enlarged pictures of marked regions within dashed boxes.

4 CONCLUSIONS

Facile and scalable protocols were successfully built to make CNT/CF/epoxy hybrids, by which void-free laminates can be manufactured. The ILFT under Mode I and Mode II loading cases were investigated and discussed comparatively, followed by a systematic analysis of failure and toughening mechanisms. The following conclusions can be reached:

Assembling micro CNTs to macro fiber veils is a promising way to fully explore the excellent properties of CNTs on a macroscopic scale. Since there is no need to disperse them into the matrix, there exists no disadvantages such as an increased viscosity or inhomogeneous dispersion which makes them suited candidates for most laminate manufacturing routes.

The results also demonstrated that the degree of densification of the CNT veil exerts a profound influence on the resulting interlaminar properties. Low-density “fluffy” CNT veils consistently led to CFRP laminates with as much as 60% enhancement of Mode I ILFT. In contrast, integrating densified CNT veils deteriorated their interlaminar mechanical performances. This layer functioned essentially as a defect that weakened the interlaminar region and did not produce any fiber-bridging, thus effectively reducing the fracture toughness of resulting laminate.

Interleaving as-produced fluffy CNT veils into unidirectional CFRP system led to an increase of Mode II ILFT (22%) but a significant decrease of Mode I ILFT (-64%). It is common for a same interleaving system varies dramatically in Mode I and Mode II toughening effects because of totally different stress state under respective mode, with Mode I being dominated by peel forces and Mode II being dominated by shear forces.

ACKNOWLEDGEMENTS

The authors are grateful for generous financial support provided by the European Union Seventh Framework Program under grant agreement 678565 (ERC-STEM), the SORCERER "Structural power composites for future civil aircraft" (Grant No. 738085), the MINECO (RyC-2014-15115, MAT2015-64167-C2-1-R), the ESTENEA funded by AIRBUS Operations S.L. and CDTI (CIEN 2014 program), and the Cost Action CA15107 (MultiComp). Yunfu Ou appreciates the financial support from the China Scholarship Council [grant number 201606130061].

REFERENCES

[1] R. Guzman de Villoria, P. Hallander, L. Ydrefors, P. Nordin, and B. Wardle, In-plane strength enhancement of laminated composites via aligned carbon nanotube interlaminar reinforcement, *Composites Science and Technology*, **133**, 2016, pp. 33-39 (doi: 10.1016/j.compscitech.2016.07.006).

[2] H. Qian, E. S. Greenhalgh, M. S. Shaffer, and A. Bismarck, Carbon nanotube-based hierarchical composites: a review, *Journal of Materials Chemistry*, **20**, 2010, pp. 4751-4762 (doi: 10.1039/c000041h).

[3] F. H. Gojny, M. H. Wichmann, B. Fiedler, and K. Schulte, Influence of different carbon nanotubes on the mechanical properties of epoxy matrix composites–a comparative study, *Composites Science and Technology*, **65**, 2005, pp. 2300-2313 (doi: 10.1016/j.compscitech.2005.04.021).

[4] S. van der Heijden, L. Daelemans, B. De Schoenmaker, I. De Baere, H. Rahier, W. Van Paepegem, *et al.*, Interlaminar toughening of resin transfer moulded glass fibre epoxy laminates by polycaprolactone electrospun nanofibres, *Composites Science and Technology*, **104**, 2014, pp. 66-73 (doi: 10.1016/j.compscitech.2014.09.005).

[5] Y. Li, I. A. Kinloch, and A. H. Windle, Direct spinning of carbon nanotube fibers from chemical vapor deposition synthesis, *Science*, **304**, 2004, pp. 276-278 (doi: 10.1126/science.1094982).

[6] ASTM Standard D5528, Standard Test Method for the Mode I Interlaminar Fracture Toughness of Unidirectional Fiber-Reinforced Polymer Matrix Composites, 2013.

[7] A. Arrese and F. Mujika, Influence of bending rotations on three and four-point bend end notched flexure tests, *Engineering Fracture Mechanics*, **75**, 2008, pp. 4234-4246.

[8] A. F. Gill, P. Robinson, and S. Pinho, Effect of variation in fibre volume fraction on modes I and II delamination behaviour of 5HS woven composites manufactured by RTM, *Composites Science and Technology*, **69**, 2009, pp. 2368-2375 (doi: 10.1016/j.compscitech.2009.02.008).

[9] L. Daelemans, S. van der Heijden, I. De Baere, H. Rahier, W. Van Paepegem, and K. De Clerck, Nanofibre bridging as a toughening mechanism in carbon/epoxy composite laminates interleaved with electrospun polyamide nanofibrous veils, *Composites Science and Technology*, **117**, 2015, pp. 244-256 (doi: 10.1016/j.compscitech.2015.06.021).

[10] F. Narducci, K.-Y. Lee, and S. Pinho, Interface micro-texturing for interlaminar toughness tailoring: a film-casting technique, *Composites Science and Technology*, **156**, 2018, pp. 203-214 (doi: 10.1016/j.compscitech.2017.10.016).

[11] J. Heremans, I. Rahim, and M. Dresselhaus, Thermal conductivity and Raman spectra of carbon fibers, *Physical Review B*, **32**, 1985, p. 6742 (doi: 10.1007/s10765-017-2275-x).

[12] H. Zhang, Y. Liu, M. Kuwata, E. Bilotti, and T. Peijs, Improved fracture toughness and integrated damage sensing capability by spray coated CNTs on carbon fibre prepreg, *Composites Part A: Applied Science and Manufacturing*, **70**, 2015, pp. 102-110 (doi: 10.1016/j.compositesa.2014.11.029).

[13] K. Kepple, G. Sanborn, P. Lacasse, K. Gruenberg, and W. Ready, Improved fracture toughness of carbon fiber composite functionalized with multi walled carbon nanotubes, *Carbon*, **46**, 2008, pp. 2026-2033 (doi: 10.1016/j.carbon.2008.08.010).

[14] Y. Ou, C. González, and J. J. Vilatela, Understanding interlaminar toughening mechanisms in structural carbon fiber/epoxy composites interleaved with CNT veils, *Proceeding of ECCM18 Conference., Athens, July, 2018.*

[15] L. Carlsson, J. Gillespie Jr, and R. Pipes, On the analysis and design of the end notched flexure (ENF) specimen for mode II testing, *Journal of composite materials*, **20**, 1986, pp. 594-604 (doi: 10.1177/002199838602000606).

[16] L. K. Jain, K. A. Dransfield, and Y.-W. Mai, On the effects of stitching in CFRPs—II. Mode II delamination toughness, *Composites Science and Technology*, **58**, 1998, pp. 829-837 (doi: 10.1016/S0266-3538(97)00186-3).

[17] R. Martin and B. Davidson, Mode II fracture toughness evaluation using four point bend, end notched flexure test, *Plastics, Rubber and Composites*, **28**, 1999, pp. 401-406 (doi: 10.1179/146580199101540565).

[18] C. Schuecker and B. D. Davidson, Evaluation of the accuracy of the four-point bend end-notched flexure test for mode II delamination toughness determination, *Composites Science and Technology*, **60**, 2000, pp. 2137-2146 (doi: 10.1016/S0266-3538(00)00113-5).